#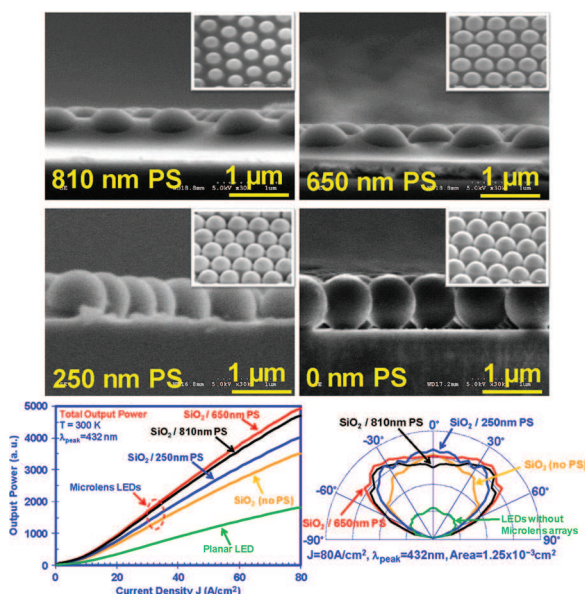 Light Extraction Efficiency and Radiation Patterns of III-Nitride Light-Emitting Diodes With Colloidal Microlens Arrays With Various Aspect Ratios

Xiao-Hang Li, Student Member, IEEE
Renbo Song
Yik-Khoon Ee
Pisist Kumnorkaew
James F. Gilchrist
Nelson Tansu, Senior Member, IEEE

Light Extraction Efficiency and Radiation Patterns of III-Nitride Light-Emitting Diodes With Colloidal Microlens Arrays With Various Aspect Ratios

Xiao-Hang Li,[1] *Student Member, IEEE*, Renbo Song,[1]
Yik-Khoon Ee,[1] Pisist Kumnorkaew,[2] James F. Gilchrist,[2] and
Nelson Tansu,[1] *Senior Member, IEEE*

[1]Center for Optical Technologies, Department of Electrical and Computer Engineering,
Lehigh University, Bethlehem, PA 18015 USA
[2]Department of Chemical Engineering, Center for Advanced Materials and Nanotechnology,
Lehigh University, Bethlehem, PA 18015 USA

Abstract: The fabrication studies of silica/polystyrene (PS) colloidal microlens arrays with various aspect ratios were performed on the III-nitride light-emitting diodes (LEDs). The use of colloidal-based microlens arrays led to significant enhancement in light extraction efficiency for III-nitride LEDs. In varying the aspect ratios of the microlens arrays, the engineering of various PS thicknesses was employed by using high-temperature treatment and redeposition process. The effects of PS thickness on the light extraction efficiency and far-field emission patterns of InGaN quantum-well (QW) LEDs were studied. The total output powers of microlens LEDs with various PS thicknesses exhibited 1.93–2.70 times enhancement over that of planar LEDs, and the use of optimized PS layer thickness is important in leading the enhancement of the light extraction efficiency in large angular direction.

Index Terms: III-Nitrides, light-emitting diodes (LEDs), light extraction efficiency, microlens arrays, far-field radiation.

1. Introduction

In addition to various applications for lasers [1]–[7], thermoelectric [8]–[11], photovoltaics and solar energy conversion [12]–[14], and terahertz photonics [15], III-nitride compound semiconductors are of great importance for light-emitting diodes (LEDs) employed in solid-state lighting [16]–[30]. One of the major challenges related to conventional III-nitride LEDs is the narrow photon escape cone (23.5°) and, thus, low light extraction efficiency (4%) due to the large refractive index contrast between GaN (n = 2.5) and free space (n = 1.0). Various approaches have been used to enhance the light extraction efficiency for III-nitride LEDs, such as surface roughening [31]–[34], sapphire microlenses [35], oblique mesa sidewalls [36], nanopyramids [37], photonic crystals [38]–[41], graded refractive index materials [42], [43], and self-assembled lithography p-GaN patterning [44].

The sapphire microlenses and photonic crystals approaches utilize either e-beam lithography or holography lithography, while the other approaches such as surface roughening employs chemical
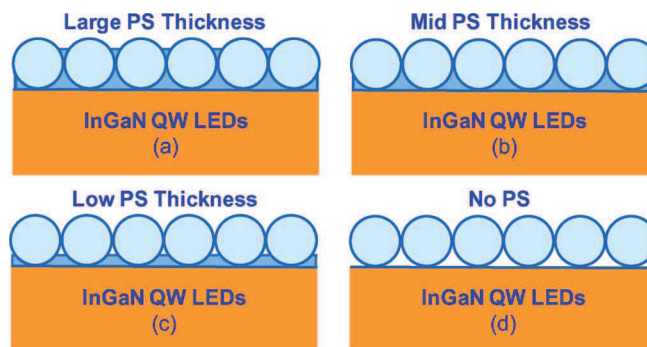
Fig. 1. (a)–(d) Cross-sectional schematics of SiO$_2$/PS microlens arrays on InGaN QW LEDs with various PS thicknesses. The ability to tune the PS thickness with high-temperature treatment resulted in convex microlens with various aspect ratios.

etching. Thus, the issues of nonuniformity or high cost are associated with these processes, which impede the large-scale and low-cost production applicable for LEDs. Hence, approaches based on inexpensive, amenable and large-scale methods for enhancing the light extraction efficiency of LEDs are highly desirable for commercialization.

The refractive indices of SiO$_2$ and polystyrene (PS) in the visible spectrum are 1.58 and 1.46, respectively. Hence, the SiO$_2$/PS monolayer microlens arrays on the planar emitting surface of LEDs can provide graded refractive index transition and convex lens shape between GaN and air. Thus, the light extraction efficiency of LEDs can be increased due to the reduced Fresnel reflection, enlarged photon escape cone and enhanced photon scattering. Our recent works based on a low-cost approach for enhancing the light extraction efficiency by depositing self-assembled 2-D close-packed and large-scale SiO$_2$/PS microlens arrays on the GaN emitting surface of LEDs were demonstrated [45]–[47]. However, the fabrication of SiO$_2$/PS microlens arrays with various PS thicknesses, as well as the impact of the PS thicknesses on the extraction efficiency and far-field pattern of LEDs has not been studied. In addition to the convex microlens arrays approach [45]–[47], the use of PDMS concave microlens arrays to increase nitride LED light extraction efficiency was recently demonstrated [48].

In this paper, we present detailed fabrication studies of self-assembled 2-D close-packed and large-scale SiO$_2$/PS microlens arrays with various PS thicknesses on top-emitting InGaN quantum well (QW) LEDs. The SiO$_2$/PS microlens array deposition is accomplished by employing the rapid convective deposition (RCD) [45]–[47]. The diameter of SiO$_2$ microspheres was fixed at 1.0 μm, and the thickness of the PS layer can be tuned from 0 nm to 810 nm with high-temperature (140 °C) treatment and redeposition process. The electroluminescence (EL) output-power versus current density measurements in the normal direction were carried to investigate the light extraction efficiencies of the LEDs with SiO$_2$/PS microlens arrays with different PS thicknesses. The LED far-field EL measurements were also performed to understand the influence of PS layer thickness on the far-field emission patterns and total output power.

2. Deposition of SiO$_2$/PS Microlens Arrays by RCD

The depositions of SiO$_2$/PS microlens arrays were performed on GaN-based top-emitting LED device structure by employing RCD process. The details of the SiO$_2$/PS microlens arrays deposition by RCD approach are available in [45]–[47]. Here, the current studies focused on fabrication of SiO$_2$/PS microlens arrays with various PS thicknesses. The ability to tune the PS layer thickness by employing high-temperature treatment leads to the ability to form SiO$_2$/PS microlens with various convex lens aspect ratios, as shown in Fig. 1(a)–(d). By embedding SiO$_2$ microspheres arrays in PS layers with different thicknesses [see Fig. 1(a)–(d)], the extraction efficiency and far-field emission patterns of the LED devices can be enhanced and optimized over the LED devices with only SiO$_2$ microsphere arrays with no PS layer.
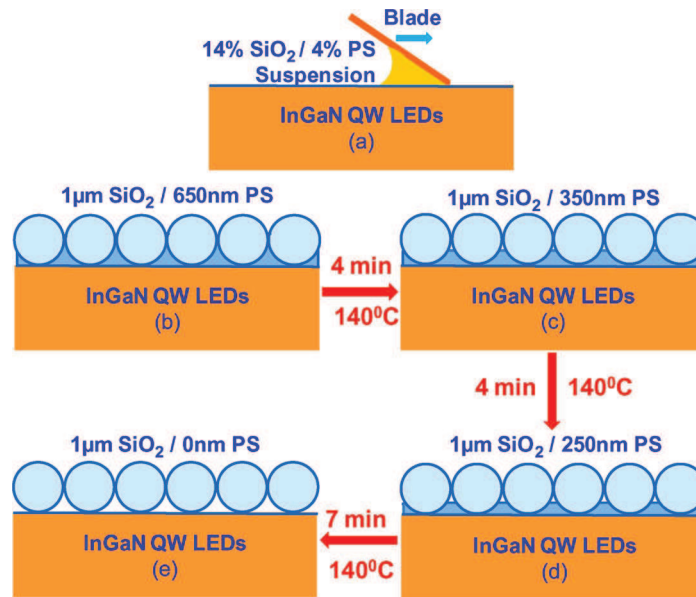
Fig. 2. (a) Cross-sectional schematics of the RCD of SiO$_2$/PS microlens arrays on top-emitting LEDs and (b)–(e) fabrication process flows of SiO$_2$/PS microlens LEDs with various PS thicknesses via high-temperature annealing at 140 °C.

In order to form microlens arrays with various aspect ratios [see Fig. 1(a)–(d)], the fabrication process of the microlens arrays were shown in Fig. 2(a)–(e). Fig. 2(a)–(e) shows the fabrication process flow of SiO$_2$/PS microlens arrays with PS thickness equal to or smaller than 650 nm via the RCD of 14% SiO$_2$/4% PS binary suspension on the LEDs. The RCD was performed in the class-1000 clean room to ensure clean surface morphology. Prior to RCD, standard optical lithography was used to cover the n- and p-metal contacts of the LEDs by photoresist (Shipley 1813), such that the SiO$_2$/PS microlens on the metal contact regions can be lifted off after the microlens deposition. The 14% SiO$_2$/4% PS binary suspension was prepared by dispersing the 1.0-μm diameter SiO$_2$ microspheres and 100-nm diameter PS nanospheres into DI-water. Afterwards, the suspension was immersed in the ultrasonic bath for 1 hour and then thoroughly shaken by the vortex for 1 min.

Fig. 2(a) shows that during the RCD, a 5.0-μL droplet SiO$_2$/PS binary suspension was firstly injected between the LED and a microscope glass slide (blade) forming a wedge with the sample at the angle of 55°. Afterwards, the blade swept across the fixed sample at a speed of 62.5 μm/s by a linear motor. Fig. 2(b) shows that after the RCD, the sample was heated at 140 °C for 1 min to melt PS nanospheres, which led to filling up the gap between the SiO$_2$ microspheres and forming a 650-nm thick planar PS layer [see Fig. 2(b)]. Thus, this process leads to forming a planar PS layer surrounding the SiO$_2$ microspheres without influencing the close-packed structure. It is important to note that the temperature of heat treatment cannot be too high, since the common photoresists may convert from novolac resins to the bakelite materials at higher temperature (200 °C for Shipley s1800 series) which can be hardly lifted off. In order to reduce the thickness of planar layer, further high-temperature annealing at 140 °C [see Fig. 2(c)–(e)] was employed onto the SiO$_2$/PS microlens LEDs with PS thickness of 650 nm. The annealing melted the 100-nm PS nanospheres and led to evaporation of PS under continuous heating. By controlling the annealing time, varying PS thicknesses were attained.

As shown in Fig. 3, the PS thickness in the SiO$_2$/PS microlens arrays is in quasi-linear proportion to the annealing time at the annealing temperature of 140 °C. Hence, arbitrary PS thicknesses between 0 nm to 650 nm can be obtained, depending on the dimension of interest. It is important to note that the melting point of bulk PS material is 240 °C that is much higher than the annealing temperature of 140 °C. However, Karabacak et $al.$ reported that the nanoscale materials possess
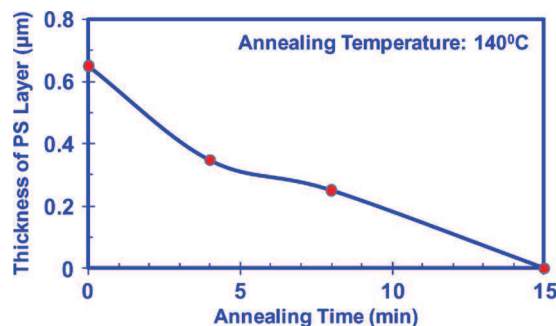
Fig. 3. PS thickness versus annealing time of SiO_2/PS microlens arrays deposited by the RCD of 14% SiO_2/4% PS binary suspension.

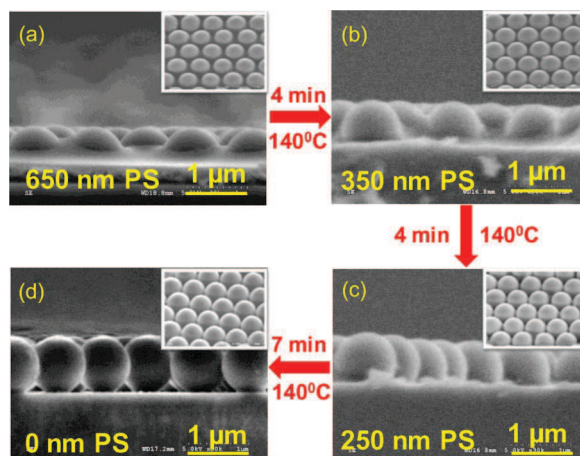Fig. 4. SEM images for the 1.0-μm SiO_2/PS microlens arrays LEDs with PS thicknesses of (a) 650 nm, (b) 350 nm, (c) 250 nm, (d) 0 nm, with the insets showing the images tilted at 45°.

significantly lower melting points than those of bulk materials due to enlarged surface area [49]. In this paper, the diameter of PS nanospheres is 100 nm, which led to a melting point below 100 °C as observed in our experiments. Further increase in annealing temperature is believed to encourage faster evaporation. The annealing temperature of 140 °C was chosen for the consistency with our previous studies [45]–[47].

To investigate the surface topographies and planar PS thickness of SiO_2/PS microlens arrays, the scanning electron microscopy (SEM) [Hitachi 4300] experiments were performed after RCD and annealing [see Fig. 2(a)–(e)]. Fig. 4(a)–(d) shows cross-sectional and 45°-tilted SEM images of the SiO_2/PS microlens arrays on top of the LED with PS thicknesses of 0 nm, 250 nm, 350 nm, and 650 nm, respectively. From Fig. 4(a)–(d), the SEM images clearly indicate the fabrication of the convex microlens arrays on the GaN-based LEDs samples with various aspect ratios. As shown in Fig. 4(b), by annealing the sample at 140 °C for 4 min, the evaporation process of PS led to the reduction of PS thickness to 350 nm. The PS layer thickness can be further reduced to 250 nm with 4 additional minutes of annealing [see Fig. 4(c)]. Finally, PS layer was completely evaporated off with total annealing time of 15 min [see Fig. 4(d)].

In addition to the approach described earlier by employing single SiO_2 microspheres + PS nanospheres RCD technique, the use of second PS nanosphere RCD will provide additional degree of freedom in forming the convex microlens arrays. To achieve the 810-nm thick PS layer structure [see Fig. 5(b)], Fig. 5(a) shows that the second RCD of 4% 100-nm PS nanosphere unary suspension was performed following the first RCD of 14% SiO_2/4% PS binary suspension,
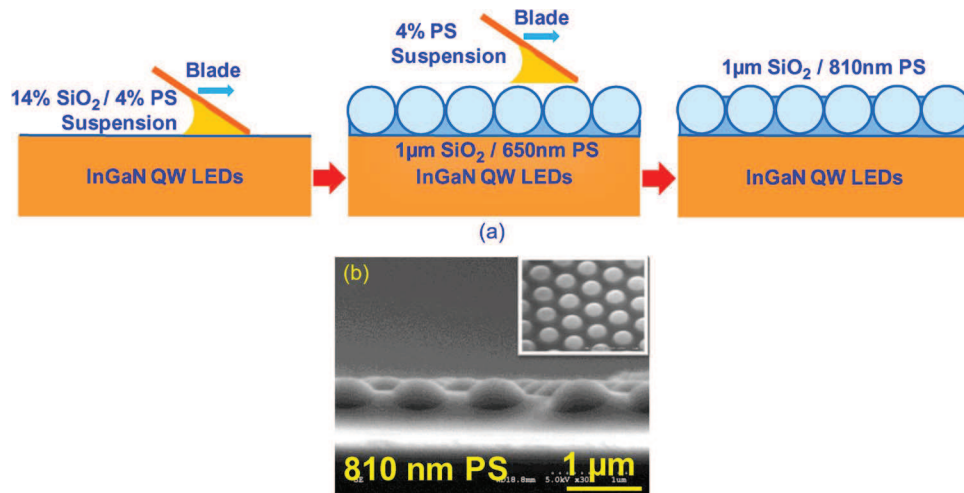
Fig. 5. (a) Fabrication process flow and (b) SEM images of SiO_2/PS coated LEDs with PS thickness of 810 nm deposited by two RCDs, with the inset showing SEM image tilted at 45°.

which led to 1.0-μm SiO_2/650-nm PS microlens arrays [see Fig. 4(a)]. Similarly, the 4% PS unary suspension was prepared by dispersing 100-nm diameter PS nanospheres into DI-water to form 4% PS unary suspension. In succession after the ultrasonic bath and vortex shaking, a 5.0 μL droplet of 4% PS unary suspension was injected between the sample and blade. The blade angle was kept at 55° but the sweeping blade speed was modified to 58.3 μm/s. Then, the sample was heated at 140 °C for 1 min to melt the PS nanospheres into the planar PS layer. As shown in Fig. 5(b), the additional PS nanospheres increased the thickness of PS planar layer to 810 nm.

From our studies, we found that the variation of volume fraction of PS nanospheres in the SiO_2/PS binary suspension could also change the PS thickness of SiO_2/PS microlens arrays, without implementing the annealing process. However, the unoptimized volume fraction of PS nanospheres can damage the close-packed property of the SiO_2/PS microlens arrays by introducing vacancies of SiO_2 microspheres [50], which hinder the enhancement of light extraction efficiency. The 4% volume fraction of PS nanospheres in the SiO_2/PS binary suspension was observed to lead to optimized RCD condition with almost no vacancies in the microlens arrays, as shown in the insets of Figs. 4(a)–(d) and 5(b). Therefore, the implementation of RCDs of binary suspension and unary suspension, and the annealing processes are more applicable in tuning the PS layer thickness.

3. Experimental Results of EL Studies for Nitride LEDs

3.1. Characteristics of Normal and Oblique Radiation Patterns

In order to characterize the light extraction efficiency enhancement of the LEDs with microlens arrays, the EL studies were performed. After the deposition of the microlens arrays, the LED samples with microlens arrays were immersed into the photoresist developer Shipley 351 at 60 °C to lift off the photoresist. It is important to note that acetone could not be used for lifting off the photoresist in this study since acetone dissolves PS very well. All the LEDs in this study here were grown on 3.0-μm thick n-GaN template on c-plane sapphire substrates by the Veeco P-75 metalorganic chemical vapor deposition (MOCVD) reactor. The active region in the LED structure consists of 4 periods of InGaN/GaN QWs with the central emitting wavelength of 432 nm. The n-GaN template was Si-doped with doping level of 5×10^{18} cm^{-3}. The p-GaN was grown utilizing 200 nm thick Mg-doped GaN with doping level of 3×10^{17} cm^{-3} at 970 °C, followed by the N_2 annealing at 850 °C. The LEDs were fabricated as top-emitting devices with the area of 1.25×10^{-3} cm^2, and Ti/Au as n-contact and Ni/Au as p-contact were evaporated followed by the rapid thermal annealing.
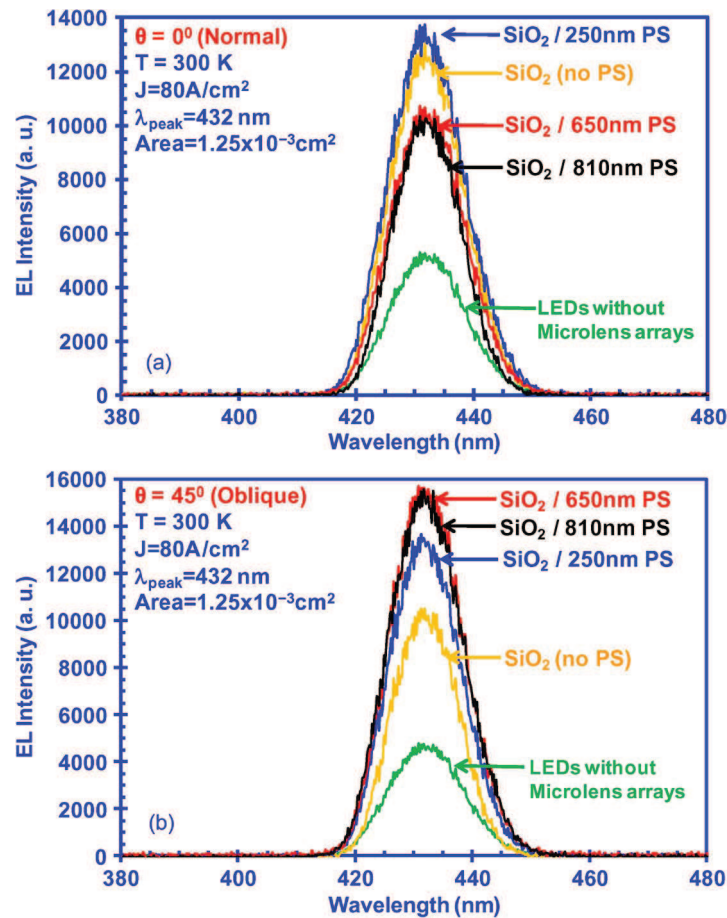
Fig. 6. Measured EL spectra of InGaN QW LEDs emitting at 432 nm of SiO_2/PS microlens LEDs with various PS thicknesses and planar LED for (a) normal direction at angle of 0° (normal to sample surface) and (b) oblique direction at angle of 45°.

The on-wafer continuous wave (CW) power measurements were performed in the dark room at room temperature for the planar LED (as reference), and SiO_2/PS microlens LEDs with PS thicknesses of 0 nm, 250 nm, 650 nm, and 810 nm, respectively. In order to ensure the consistency of LED characteristics and the accuracy of the comparison, all the measurements were conducted on the hexagonal LED device with identical mesa area of 1.25×10^{-3} cm².

Fig. 6(a) shows the EL spectra at $\theta = 0°$ (normal direction) of the planar LED and SiO_2/PS microlens LEDs with various PS thicknesses at the current density of 80 A/cm². The microlens LEDs with PS thicknesses of 0 nm, 250 nm, 650 nm, and 810 nm exhibit 2.40, 2.60, 2.03, and 1.96 times improvement in the integrated power, respectively, as opposed to that of the planar LED. Hence, the SiO_2/PS microlens arrays can lead to significant increase in light extraction efficiency in the normal direction, which is mainly due to the enlarged light escape cone and reduced Fresnel reflection.

In addition to the measurement at $\theta = 0°$ [see Fig. 6(a)], the EL spectra of the SiO_2/PS microlens LEDs were also measured at $\theta = 45°$ (oblique direction) and at the same current density of 80 A/cm², as shown in Fig. 6(b). In Fig. 6(b), the integrated powers of SiO_2/PS microlens LEDs with PS thicknesses of 0 nm, 250 nm, 650 nm, and 810 nm show 2.19, 2.80, 3.27, and 3.18 times enhancement, in comparison with that of the planar LED at the current density of 80 A/cm². It is important to note that the peak intensity of EL spectrum of microlens LEDs with PS thickness of 0 nm (yellow curve) is considerably lower than that of itself at $\theta = 0°$ and those of the other microlens LEDs at $\theta = 45°$. The peak intensities of EL spectra of microlens LEDs with PS thickness of 650 nm (yellow
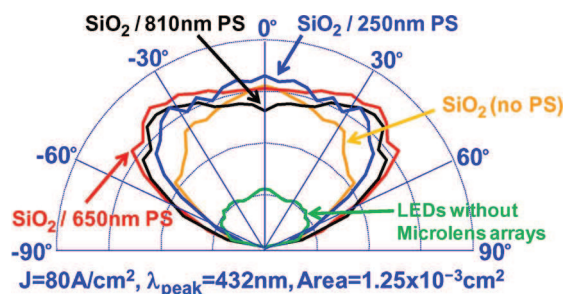
Fig. 7. Far-field emission patterns of the planar LED and SiO$_2$/PS microlens LEDs with various PS thicknesses.

curve) and 810 nm (black curve) at $\theta = 45°$ are observed to be higher at than those at $\theta = 0°$. Hence, the comparison between Fig. 6(a) and (b) indicates that the use of PS layer into SiO$_2$ microsphere arrays to form SiO$_2$/PS microlens arrays with various thicknesses lead to significant increase in the diffusion of light at large oblique angle direction.

In order to further investigate the significant difference of the EL spectrum intensities of microlens LEDs with various PS thicknesses at $\theta = 0°$ and $\theta = 45°$, the angle-dependent EL far-field studies were carried for all the LEDs studied here, as shown in Fig. 7. The far-field measurements were taken from $\theta = 0°$ up to $\theta = 90°$. Note that the results presented for $\theta = -90°$–$0°$ range are identical with those from $\theta = 0°$–$90°$ range, and both results are presented in the same plot for completeness purpose (Fig. 7). The far-field emission patterns of SiO$_2$/PS microlens LEDs were measured on the LEDs at the current density of 80 A/cm^2. The far-field measurement setup consisted of a semi-circular structure on which the optical fiber can be rotated 180° in a single plane. The measured LEDs were placed in the center of the semicircular structure, hence the optical fiber kept equidistant away from the measured LED as the optical fiber rotated through 180° in the plane to collect the emission at varying angles. As the distance between the optical fiber and measured LEDs was fixed at 2.5 cm which was much larger than the dimension of the measured LEDs (regular hexagon with edge length of 220 μm), the far-field measurement condition was fulfilled [51]. As shown in Fig. 7, the output power of the emission is radially plotted, with 0° as normal to the LED emitting surface. Fig. 7 shows that all the far-field emission patterns exhibit Lambertian-like radiation patterns attributed to the large index contrast between GaN and free space. The far-field emission patterns of LEDs with microlens arrays show considerably stronger radiant intensity over that of the planar LED. Both the normal direction and large angle far-field pattern for LEDs with microlens arrays exhibit significant enhancement over those of the planar LED, which is attributed to reduced Fresnel reflection and enlarged escape cone. In addition, the use of PS layer in the SiO$_2$/PS microlens LEDs is important in particular for enhancing the light extraction efficiency in the large oblique angle direction, leading to more diffused far-field pattern (see Fig. 7).

From Fig. 7, the measured far-field emission of the SiO$_2$/PS microlens LEDs was much larger than that of the planar LED. However, the enhancement ratios of the far-field emission as a function of angular direction vary significantly for SiO$_2$/PS microlens LEDs with various PS thicknesses. As shown in Fig. 8, the far-field emission intensities of the SiO$_2$/PS microlens LEDs were normalized to that of the planar LED in order to obtain the enhancement ratios of output power as a function of angular distribution. The enhancement ratios of the SiO$_2$/PS microlens LED with PS thickness of 0 nm are more significant at small angles from 0° to 30° than that at larger angles. However, the implementation of the PS layer in the SiO$_2$/PS microlens LEDs for PS thicknesses of 250 nm, 650 nm, and 810 nm greatly enhanced the far-field emission at larger angular distribution in particular at 30° up to 50°. The use of SiO$_2$/PS microlens LED with PS thickness of 650 nm led to the largest far-field emission ratio at large angular distribution. At $\theta = 45°$ where the EL spectra of the LEDs were measured [see Fig. 6(b)], the enhancement ratio of output power of the microlens LED with PS thickness of 0 nm is significantly lower than those of microlens LEDs with PS layers. Thus, our finding indicate that the use of microlens with optimized PS thickness led to enhancement in light extraction
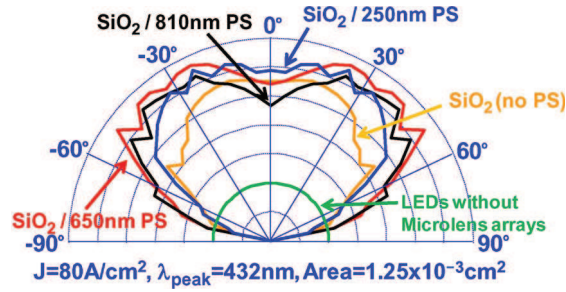
Fig. 8. Far-field emission enhancement ratio of output power as a function of far-field angle for LEDs with microlens arrays normalized to that of planar LEDs.
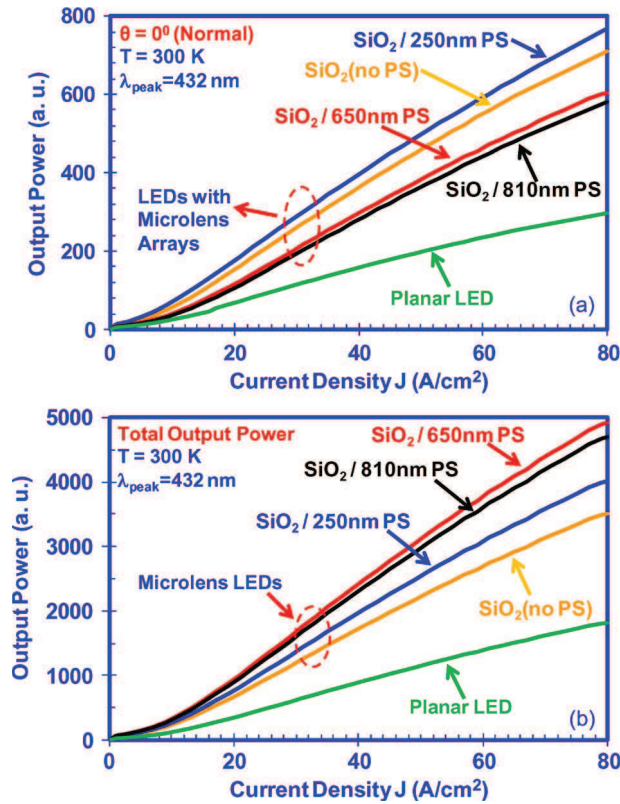

Fig. 9. Light output power versus current density of InGaN QW LEDs employing SiO_2/PS microlens arrays with various PS thicknesses for (a) normal direction at angle of $0°$ (normal to sample surface) and (b) total output power integrated over all angular directions. The EL measurement data for planar LEDs without microlens arrays are presented for comparison.

efficiency due to the increase in the light extraction in the large angular direction, which corresponded to the diffuse light enhancement.

3.2. Comparison of Light Output Powers Versus Current Density

In order to study the relationship between the output powers of SiO_2/PS microlens LEDs versus the injected current density, the output power measurements were carried out under CW operation. Fig. 9(a) shows the output powers as a function of the current density up to 80 A/cm^2 for normal direction ($\theta = 0°$). The output powers show quasi-linear relation with increasing current density, and
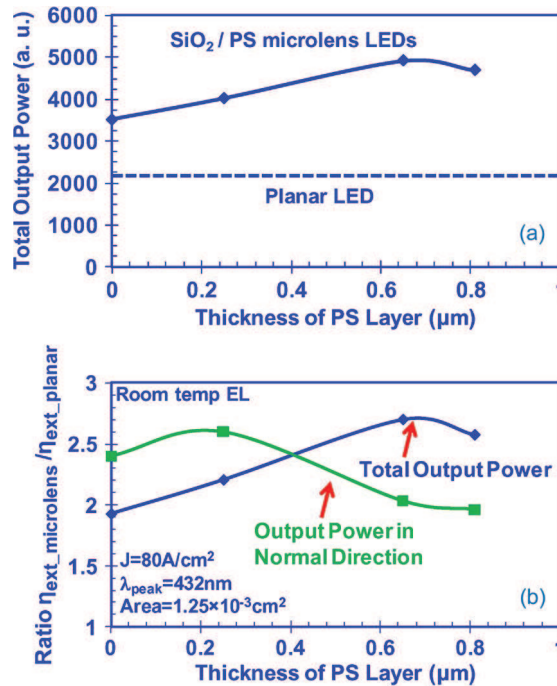
Fig. 10. (a) Total output power versus PS thickness of the SiO_2/PS coated LEDs (solid curve) and planar LED (dash line) and (b) the external efficiency enhancement ratios from total output power and output power in normal direction for SiO_2/PS coated LEDs with various PS thicknesses.

the results also indicated evidence of efficiency droop at high current density. As exhibited in Fig. 9(a), at the current density of 80 A/cm², the EL measurements show 2.40, 2.60, 2.03, and 1.96 times improvement in the output powers of the SiO_2/PS microlens LEDs with PS thicknesses of 0 nm, 250 nm, 650 nm, and 810 nm, respectively, in comparison with that of the planar LED, similar to the finding in Fig. 6(a).

Note that the far-field measurements [see Figs. 7 and 8] indicate that the implementation of the SiO_2/PS microlens LEDs with PS layer leads to stronger far-field enhancement at higher angles, in comparison to the SiO_2/PS microlens LEDs with no PS layer. Thus, the integrated output powers of the LEDs were obtained by integrating the far-field output power across all solid angles, as shown in Fig. 9(b). Fig. 9(b) plots the total output powers as a function of the current density up to 80 A/cm². The total output powers of the microlens LEDs with PS thicknesses of 0 nm, 250 nm, 650 nm, and 810 nm exhibit 1.93, 2.21, 2.70, and 2.57 times enhancement, as compared with that of the planar LED at the current density of 80 A/cm². The significant enhancement in the output powers measured for LEDs employing SiO_2/PS microlens arrays with PS thicknesses of 650 nm and 810 nm can be attributed to the large diffuse light extraction in the large angular direction.

To provide comparison of the device characteristics of microlens-based LEDs and planar LED, the output powers and extraction efficiency enhancement ratios were plotted. Fig. 10(a) shows the total output powers versus PS thickness of SiO_2/PS microlens LEDs and total output power of the planar LED at the current density of 80 A/cm². The ratios of the light extraction efficiency for the integrated powers over all angular directions for the LEDs with microlens arrays over that of planar LEDs were shown in Fig. 10(b). In comparison, the ratios of the output powers in normal direction for the microlens LEDs and planar LEDs were plotted as well in Fig. 10(b). From the results in Fig. 10(a) and (b), it is evident that the implementation of the optimized PS layer thickness in the SiO_2/PS microlens arrays led to enhancement in the output power and light extraction efficiency, in particular in enhancing the diffuse light extraction at large angular direction. This comparison supports the observation in the EL measurements that the controllability of PS layer thickness is critical in extracting and diffusing the light toward the larger angular directions.

4. Summary

In summary, the optimization studies of the self-assembled 2-D close-packed SiO_2/PS microlens with various PS thicknesses were performed by employing the RCD and high-temperature (140 °C) treatment. The fabrication of the colloidal microlens arrays with various aspect ratios was carried out for III-nitride LEDs applications. Both the EL in the normal direction and far-field measurements were carried out on III-nitride LEDs with these microlens arrays. The engineering of the PS layer thickness is important in increasing the light extraction (1.93 to 2.70 times) and achieving more diffusive radiation pattern in particular at large angular direction from 30° to 50°, which showed the compatibility of this approach for solid state lighting applications.

References

[1] R. M. Farrell, D. F. Feezell, M. C. Schmidt, D. A. Haeger, K. M. Kelchner, K. Iso, H. Yamada, M. Saito, K. Fujito, D. A. Cohen, J. S. Speck, P. DenBaars, and S. Nakamura, "Continuous-wave operation of AlGaN-cladding-free nonpolar m-plane InGaN/GaN laser diodes," *Jpn. J. Appl. Phys.*, vol. 46, no. 32, pp. L761–L763, Aug. 2007.

[2] D. Sizov, R. Bhat, J. Napierala, C. Gallinat, K. Song, D. Allen, and C. E. Zah, "Optical gain and gain saturation of blue-green InGaN quantum wells," *Physica Status Solidi A*, vol. 207, no. 6, pp. 1309–1312, Jun. 2010.

[3] H. Yoshida, M. Kuwabara, Y. Yamashita, K. Uchiyama, and H. Kan, "Radiative and nonradiative recombination in an ultraviolet GaN/AlGaN multiple-quantum-well laser diode," *Appl. Phys. Lett.*, vol. 96, no. 21, pp. 211122-1–211122-3, May 2010.

[4] M. Kneissl, D. W. Treat, M. Teepe, N. Miyashita, and N. M. Johnson, "Continuous-wave operation of ultraviolet InGaN/InAlGaN multiple-quantum-well laser diodes," *Appl. Phys. Lett.*, vol. 82, no. 15, pp. 2386–2388, Apr. 2003.

[5] J. Zhang, H. Zhao, and N. Tansu, "Large optical gain AlGaN-Delta-GaN quantum wells laser active regions in mid- and deep-ultraviolet spectral regimes," *Appl. Phys. Lett.*, vol. 98, no. 17, pp. 171111-1–171111-3, Apr. 2011.

[6] M. C. Schmidt, K.-C. Kim, R. M. Farrell, D. F. Feezell, D. A. Cohen, M. Saito, K. Fujito, J. S. Speck, S. P. Denbaars, and S. Nakamura, "Demonstration of nonpolar m-plane InGaN/GaN laser diodes," *Jpn. J. Appl. Phys.*, vol. 46, no. 9, pp. L190–L191, Feb. 2007.

[7] D. Queren, A. Avramescu, G. Bruderl, A. Breidenassel, M. Schillgalies, S. Lutgen, and U. Strau, "500 nm electrically driven InGaN based laser diodes," *Appl. Phys. Lett.*, vol. 94, no. 8, pp. 081119-1–081119-3, Feb. 2009.

[8] B. N. Pantha, R. Dahal, J. Li, J. Y. Lin, H. X. Jiang, and G. Pomrenke, "Thermoelectric properties of $In_xGa_{1-x}N$ alloys," *Appl. Phys. Lett.*, vol. 92, no. 4, pp. 042112-1–042112-3, Jan. 2008.

[9] B. N. Pantha, R. Dahal, J. Li, J. Y. Lin, H. X. Jiang, and G. Pomrenke, "Thermoelectric properties of $In_{0.3}Ga_{0.7}N$ alloys," *J. Electron. Mater.*, vol. 38, no. 7, pp. 1132–1135, Feb. 2009.

[10] H. Tong, J. Zhang, G. Y. Liu, J. A. Herbsommer, G. S. Huang, and N. Tansu, "Thermoelectric properties of lattice-matched AlInN alloy grown by metal organic chemical vapor deposition," *Appl. Phys. Lett.*, vol. 97, no. 11, pp. 112105-1–112105-3, Sep. 2010.

[11] J. Zhang, H. Tong, G. Liu, J. A. Herbsommer, G. S. Huang, and N. Tansu, "Characterizations of seebeck coefficients and thermoelectric figures of merit for AlInN alloys with various in-contents," *J. Appl. Phys.*, vol. 109, no. 5, pp. 053706-1–053706-6, Mar. 2011.

[12] C. J. Neufeld, N. G. Toledo, S. C. Cruz, M. Iza, S. P. DenBaars, and U. K. Mishra, "High quantum efficiency InGaN/GaN solar cells with 2.95 eV band gap," *Appl. Phys. Lett.*, vol. 93, no. 14, pp. 143502-1–143502-3, Oct. 2008.

[13] R. Dahal, B. Pantha, J. Li, J. Y. Lin, and H. X. Jiang, "InGaN/GaN multiple quantum well solar cells with long operating wavelengths," *Appl. Phys. Lett.*, vol. 94, no. 6, pp. 063505-1–063505-3, Feb. 2009.

[14] O. Jani, I. Ferguson, C. Honsberg, and S. Kurtz, "Design and characterization of GaN/InGaN solar cells," *Appl. Phys. Lett.*, vol. 91, no. 13, pp. 132117-1–132117-3, Sep. 2007.

[15] G. Sun, G. Xu, Y. J. Ding, H. Zhao, G. Liu, J. Zhang, and N. Tansu, "Efficient terahertz generation from multiple InGaN/GaN quantum wells," *IEEE J. Sel. Topics Quantum Electron.*, vol. 17, no. 1, pp. 48–53, Jan./Feb. 2011.

[16] M. H. Crawford, "LEDs for solid-state lighting: Performance challenges and recent advances," *IEEE J. Sel. Topics Quantum Electron.*, vol. 15, no. 4, pp. 1028–1040, Jul./Aug. 2009.

[17] G. Liu, H. Zhao, J. Zhang, J. H. Park, L. J. Mawst, and N. Tansu, "Selective area epitaxy of ultra-high density InGaN quantum dots by Diblock copolymer," *Nanoscale Res. Lett.*, vol. 6, Art. 342, Apr. 2011, DOI:10.1186/1556-276X-6-342.

[18] D. D. Koleske, A. J. Fische, A. A. Allerman, C. C. Mitchell, K. C. Cross, S. R. Kurtz, J. J. Figiel, K. W. Fullmer, and W. G. Breiland, "Improved brightness of 380 nm GaN light emitting diodes through intentional delay of the nucleation island coalescence," *Appl. Phys. Lett.*, vol. 81, no. 11, pp. 1940–1942, Sep. 2002.

[19] Y. K. Ee, J. M. Biser, W. Cao, H. M. Chan, R. P. Vinci, and N. Tansu, "Metalorganic vapor phase epitaxy of III-nitride light-emitting diodes on nano-patterned AGOG sapphire substrate by abbreviated growth mode," *IEEE J. Sel. Topics Quantum Electron.*, vol. 15, no. 4, pp. 1066–1072, Jul./Aug. 2009.

[20] T. Jung, L. K. Lee, and P. C. Ku, "Novel epitaxial nanostructures for the improvement of InGaN LEDs efficiency," *IEEE J. Sel. Topics Quantum Electron.*, vol. 15, no. 4, pp. 1073–1079, Jul./Aug. 2009.

[21] H. Zhao, J. Zhang, G. Liu, and N. Tansu, "Surface plasmon dispersion engineering via double-metallic Au/Ag layers for III-nitride based light-emitting diodes," *Appl. Phys. Lett.*, vol. 98, no. 15, pp. 151115-1–151115-3, Apr. 2011.

[22] X. Li, S. G. Bishop, and J. J. Coleman, "GaN epitaxial lateral overgrowth and optical characterization," *Appl. Phys. Lett.*, vol. 73, no. 9, pp. 1179–1181, Aug. 1998.

[23] X. Li, S. Kim, E. E. Reuter, S. G. Bishop, and J. J. Coleman, "The Incorporation of Arsenic in GaN by Metalorganic Chemical Vapor Deposition," *Appl. Phys. Lett.*, vol. 72, no. 16, pp. 1990–1992, Apr. 1998.

[24] C. T. Liao, M. C. Tsai, B. T. Liou, S. H. Yen, and Y. K. Kuo, "Improvement in output power of a 460 nm InGaN light-emitting diode using staggered quantum well," *J. Appl. Phys.*, vol. 108, no. 6, pp. 063107-1–063107-6, Sep. 2010.

[25] H. P. Zhao, G. Y. Liu, X. H. Li, R. A. Arif, G. S. Huang, J. D. Poplawsky, S. Tafon Penn, V. Dierolf, and N. Tansu, "Design and characteristics of staggered InGaN quantum well light-emitting diodes in the green spectral regimes," *IET Optoelectron.*, vol. 3, no. 6, pp. 283–295, Dec. 2009.

[26] S. H. Park, D. Ahn, B. H. Koo, and J. W. Kim, "Dip-shaped InGaN/GaN quantum-well light-emitting diodes with high efficiency," *Appl. Phys. Lett.*, vol. 95, no. 6, pp. 063507-1–063507-3, Aug. 2009.

[27] S. H. Park, D. Ahn, and J. W. Kim, "High-efficiency staggered 530 nm InGaN/InGaN/GaN quantum-well light-emitting diodes," *Appl. Phys. Lett.*, vol. 94, no. 4, pp. 041109-1–041109-3, Jan. 2009.

[28] N. F. Gardner, G. O. Muller, Y. C. Shen, G. Chen, S. Watanabe, W. Gotz, and M. R. Krames, "Blue-emitting InGaN–GaN double-heterostructure light-emitting diodes reaching maximum quantum efficiency above 200A/cm^2," *Appl. Phys. Lett.*, vol. 91, no. 24, pp. 243506-1–243506-3, Dec. 2007.

[29] M. F. Schubert, J. Xu, J. K. Kim, E. F. Schubert, M. H. Kim, S. Yoon, S. M. Lee, C. Sone, T. Sakong, and Y. Park, "Polarization-matched GaInN/AlGaInN multi-quantum-well light-emitting diodes with reduced efficiency droop," *Appl. Phys. Lett.*, vol. 93, no. 4, pp. 041102-1–041102-3, Jul. 2008.

[30] H. Zhao, G. Liu, R. A. Arif, and N. Tansu, "Current injection efficiency quenching leading to efficiency droop in InGaN quantum well light-emitting diodes," *Solid State Electron.*, vol. 54, no. 10, pp. 1119–1124, Oct. 2010.

[31] C. Huh, K. S. Lee, E. J. Kang, and S. J. Park, "Improved light-output and electrical performance of InGaN-based light-emitting diode by microroughening of the p-GaN surface," *J. Appl. Phys.*, vol. 93, no. 11, pp. 9383–9385, Jun. 2003.

[32] T. Fujii, Y. Gao, R. Sharma, E. L. Hu, S. P. DenBaars, and S. Nakamura, "Increase in the extraction efficiency of GaN-based light-emitting diodes via surface roughening," *Appl. Phys. Lett.*, vol. 84, no. 6, pp. 855–857, Feb. 2004.

[33] C. F. Lin, Z. J. Yang, J. H. Zheng, and J. J. Dai, "Enhanced light output in nitride-based light-emitting diodes by roughening the mesa sidewall," *IEEE Photon. Technol. Lett.*, vol. 17, no. 10, pp. 2038–2040, Oct. 2005.

[34] H. W. Huang, J. T. Chu, C. C. Kao, T. H. Hseuh, T. C. Lu, H. C. Kuo, S. C. Wang, and C. C. Yu, "Enhanced light output of an InGaN/GaN light emitting diode with a nano-roughened p-GaN surface," *Nanotechnol.*, vol. 16, no. 9, pp. 1844–1848, Jul. 2005.

[35] H. W. Choi, C. Liu, E. Gu, G. McConnell, J. M. Girkin, I. M. Watson, and M. D. Dawson, "GaN micro-light-emitting diode arrays with monolithically integrated sapphire microlenses," *Appl. Phys. Lett.*, vol. 84, no. 13, pp. 2253–2255, Mar. 2004.

[36] S. J. Lee, J. Lee, S. Kim, and H. Jeon, "Fabrication of reflective GaN mesa sidewalls for the application to high extraction efficiency LEDs," *Phys. Stat. Sol. (C)*, vol. 4, no. 7, pp. 2625–2628, May 2007.

[37] J. Q. Xi, H. Luo, A. J. Pasquale, J. K. Kim, and E. F. Schubert, "Enhanced light extraction in GaInN light-emitting diode with pyramid reflector," *IEEE Photon. Technol. Lett.*, vol. 18, no. 15, pp. 2347–2349, Nov. 2006.

[38] D. Kim, C. Cho, Y. Roh, H. Jeon, Y. S. Park, J. Cho, J. S. Im, C. Sone, Y. Park, W. J. Choi, and Q. Park, "Enhanced light extraction from GaN-based light-emitting diodes with holographically generated two-dimensional photonic crystal patterns," *Appl. Phys. Lett.*, vol. 87, no. 20, pp. 203508-1–203508-3, Nov. 2005.

[39] T. Kim, A. J. Danner, and K. D. Choquette, "Enhancement in external quantum efficiency of blue light-emitting diode by photonic crystal surface grating," *Electron. Lett.*, vol. 41, no. 20, pp. 1138–1139, Sep. 2005.

[40] J. J. Wierer, A. David, and M. M. Megens, "III-Nitride photonic-crystal light-emitting diodes with high extraction efficiency," *Nat. Photon.*, vol. 3, no. 3, pp. 163–169, May 2009.

[41] E. Rangel, E. Matioli, Y. S. Choi, C. Weisbuch, J. S. Speck, and E. L. Hu, "Directionality control through selective excitation of low-order guided modes in thin-film InGaN photonic crystal light-emitting diodes," *Appl. Phys. Lett.*, vol. 98, no. 8, pp. 081104-1–081104-3, Feb. 2011.

[42] Q. Xi, M. F. Schubert, J. K. Kim, E. F. Schubert, M. Chen, S. Y. Lin, W. Liu, and J. A. Smart, "Optical thin-film materials with low refractive index for broadband elimination of Fresnel reflection," *Nat. Photon.*, vol. 1, no. 3, pp. 176–179, Mar. 2007.

[43] J. K. Kim, M. F. Schubert, J. Q. Xi, F. W. Mont, and E. F. Schubert, "Enhancement of light extraction in GaInN light-emitting diodes with graded-index indium tin oxide layer," presented at the Conf. Lasers Electro-Optics/Int. Quantum Electron. Conf. (CLEO/IQEC), Baltimore, MD, Jun.1, 2007, Paper CTuI1.

[44] S. Chhajed, W. Lee, J. Cho, E. F. Schubert, and J. K. Kim, "Strong light extraction enhancement in GaInN light-emitting diodes by using self-organized nanoscale patterning of p-type GaN," *Appl. Phys. Lett.*, vol. 98, no. 7, pp. 071102-1–071102-3, Feb. 2011.

[45] Y. K. Ee, P. Kumnorkaew, R. A. Arif, J. F. Gilchrist, and N. Tansu, "Enhancement of light extraction efficiency of InGaN quantum wells light emitting diodes using SiO$_2$/polystyrene microlens arrays," *Appl. Phys. Lett.*, vol. 91, no. 22, pp. 221107-1–221107-3, Nov. 2007.

[46] Y. K. Ee, P. Kumnorkaew, R. A. Arif, H. Tong, H. Zhao, J. F. Gilchrist, and N. Tansu, "Optimization of light extraction efficiency of III-nitride LEDs with self-assembled colloidal-based microlenses," *IEEE J. Sel. Topics Quantum Electron.*, vol. 15, no. 4, pp. 1218–1225, Jul./Aug. 2009.

[47] P. Kumnorkaew, Y. K. Ee, N. Tansu, and J. F. Gilchrist, "Investigation of the deposition of microsphere monolayers for fabrication of microlens arrays," *Langmuir*, vol. 24, no. 21, pp. 12 150–12 157, Nov. 2008.

[48] Y. K. Ee, P. Kumnorkaew, R. A. Arif, H. Tong, J. F. Gilchrist, and N. Tansu, "Light extraction efficiency enhancement of InGaN quantum wells light-emitting diodes with polydimethylsiloxane concave microstructures," *Opt. Express*, vol. 17, no. 16, pp. 13 747–13 757, Aug. 2009.

[49] T. Karabacak, J. S. DeLuca, P.-I. Wang, G. A. Ten Eyck, D. Ye, G.-C. Wang, and T.-M. Lu, "Low temperature melting of copper nanorod arrays," *J. Appl. Phys.*, vol. 99, no. 6, pp. 064304-1–064304-6, Mar. 2006.

[50] P. Kumnorkaew and J. F. Gilchrist, "Effect of nanoparticle concentration on the convective deposition of binary suspensions," *Langmuir*, vol. 25, no. 11, pp. 6070–6075, Apr. 2009.

[51] I. Moreno and C. C. Sun, "Modeling the radiation pattern of LEDs," *Opt. Express*, vol. 16, no. 3, pp. 1808–1819, Jan. 2008.